

Supplementary Materials for

**Acoustofluidic black holes for multifunctional in-droplet
particle manipulation**

Pengzhan Liu, Zhenhua Tian*, Kaichun Yang, Ty Downing Naquin, Nanjing Hao, Huiyu Huang,
Jinyan Chen, Qiuxia Ma, Hunter Bachman, Peiran Zhang, Xiaohong Xu*,
Junhui Hu*, Tony Jun Huang*

*Corresponding author. Email: tian@ae.msstate.edu (Z.T.); xuxiahong@zaas.ac.cn (X.X.);
ejhhu@nuaa.edu.cn (J.H.); tony.huang@duke.edu (T.J.H.)

Published 1 April 2022, *Sci. Adv.* **8**, eabm2592 (2022)
DOI: 10.1126/sciadv.abm2592

The PDF file includes:

Section S1
Figs. S1 to S10
Tables S1 and S2
Legends for movies S1 to S3
References

Other Supplementary Material for this manuscript includes the following:

Movies S1 to S3

section S1. Details of numerical models

The governing equation for computing wave fields in the solid domain (56) is

$$-\rho\omega^2\mathbf{u} = \nabla \cdot \mathbf{S} + \mathbf{F}_V e^{i\varphi} \quad (\text{S1})$$

where ρ is the substrate density, ω is the angular frequency, \mathbf{u} is the displacement vector, \mathbf{S} is the stress tensor, \mathbf{F}_V is the volume force vector, and φ is the phase. The quadratic serendipity shape functions are used to simulate displacement fields in the Solid Mechanics interface.

The governing equation for computing acoustic pressure fields in the fluid domain (57, 58) is

$$\nabla^2 p + \left(\frac{\omega}{c_0}\right)^2 p = 0 \quad (\text{S2})$$

where p is the acoustic pressure and c_0 is the wave speed in water. The quadratic Lagrangian shape functions are used to simulate acoustic pressure fields in the Pressure Acoustics interface. Aside from the coupled droplet-substrate interface, other boundaries of the fluid domain are set to acoustic soft boundaries (59).

After computing the acoustic pressure field, the acoustic velocity \mathbf{v} in the fluid domain can be computed (57, 58) based on the equation

$$\mathbf{v} = -\frac{\nabla p}{i\omega\rho_0} \quad (\text{S3})$$

where ρ_0 is the water density. With the simulated acoustic pressure and velocity, the acoustic radiation force \mathbf{F}_{rad} applied on a single particle in the acoustic field can be computed (60) using the equation

$$\mathbf{F}_{rad} = -\nabla \left\{ \frac{4}{3} \pi R_p^3 \left[\left(-\frac{3\rho_p - 3\rho_o}{2\rho_p + \rho_o} \right) \cdot \frac{1}{2} \rho_o \langle \mathbf{v} \rangle^2 + \left(1 - \frac{\rho_o c_o^2}{\rho_p c_p^2} \right) \cdot \frac{1}{2} \frac{\langle p \rangle^2}{\rho_o c_o^2} \right] \right\} \quad (\text{S4})$$

where R_p is the particle radius, ρ_p is the particle density, and c_p is the particle material's sound speed.

The governing equations for computing acoustic streaming fields in the fluid domain are

$$\nabla \cdot \mathbf{v}_1 = 0 \quad (\text{S5})$$

$$\rho_0 (\mathbf{v}_1 \cdot \nabla) \mathbf{v}_1 = \nabla \cdot \left\{ -p_1 \mathbf{I} + \mu \left[\nabla \mathbf{v}_1 + (\nabla \mathbf{v}_1)^T \right] \right\} + \mathbf{F}_R \quad (\text{S6})$$

$$\mathbf{F}_R = -\rho_0 \langle (\mathbf{v} \cdot \nabla) \mathbf{v} + \mathbf{v} (\nabla \cdot \mathbf{v}) \rangle \quad (\text{S7})$$

where \mathbf{v}_1 is the acoustic streaming velocity, p_1 is the pressure in the fluid, μ is the dynamic viscosity of water, and \mathbf{F}_R is the body force induced by the acoustic field ($\langle \rangle$ denotes the time average over a full oscillation time period) (61, 62). The fluid flow discretization is set to P1+P1 (piecewise linear interpolation for velocity and pressure) in the Laminar Flow interface. The coupled droplet-substrate interface is set to a slip boundary (63-65), and other boundaries of the fluid domain are set to no-slip boundaries.

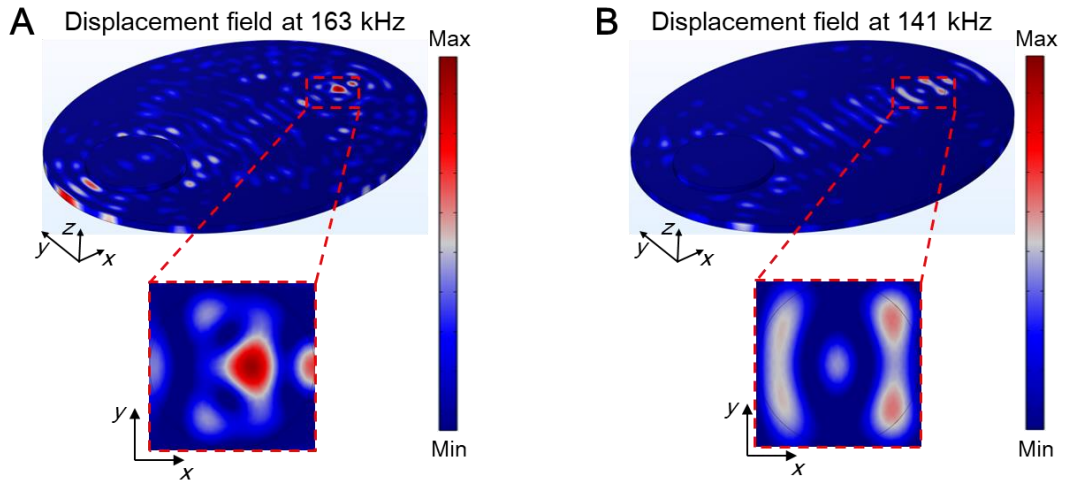


fig. S1. Simulated out-of-plane displacement amplitude fields for flexural waves generated in an elliptical substrate without an AFBH. (A) Simulation result at 163 kHz. **(B)** Simulation result at 141 kHz. These simulation results indicate the elliptical boundary can focus wideband flexural waves generated by a circular piezoelectric transducer to a region near the right focal point of the ellipse.

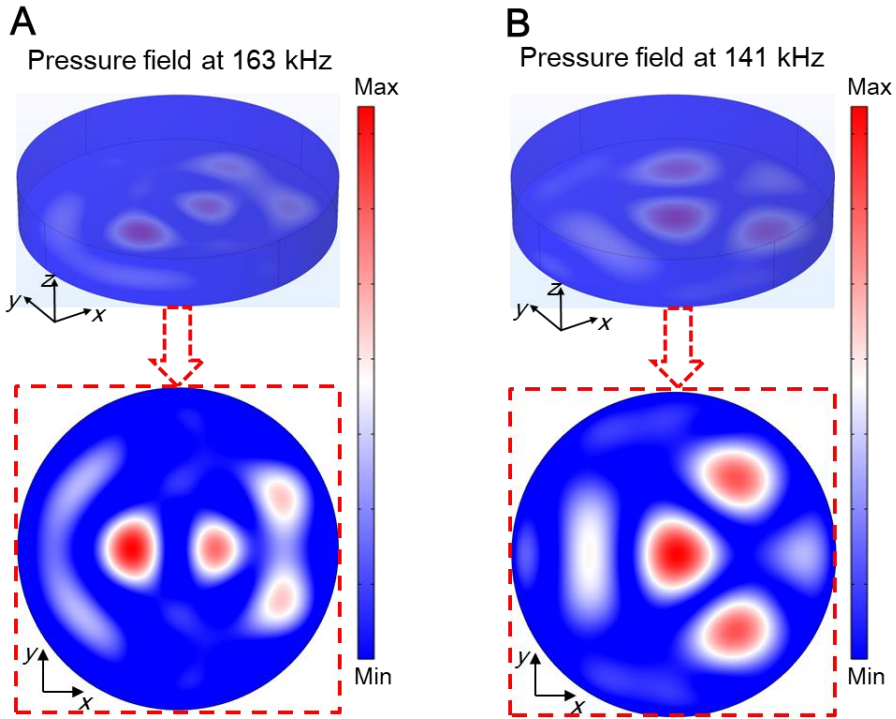


fig. S2. Simulated acoustic pressure fields in the fluid domain at different frequencies. **(A)** Simulation result at 163 kHz. **(B)** Simulation result at 141 kHz. Top row: 3D views of the simulated pressure fields. Bottom row: 2D views of the simulated pressure fields at the fluid-solid interface. These simulation results indicate that our AFBH can change in-droplet pressure fields and pressure antinode numbers by altering excitation frequencies. These features allow our AFBH-based device to achieve different in-droplet particle distributions.

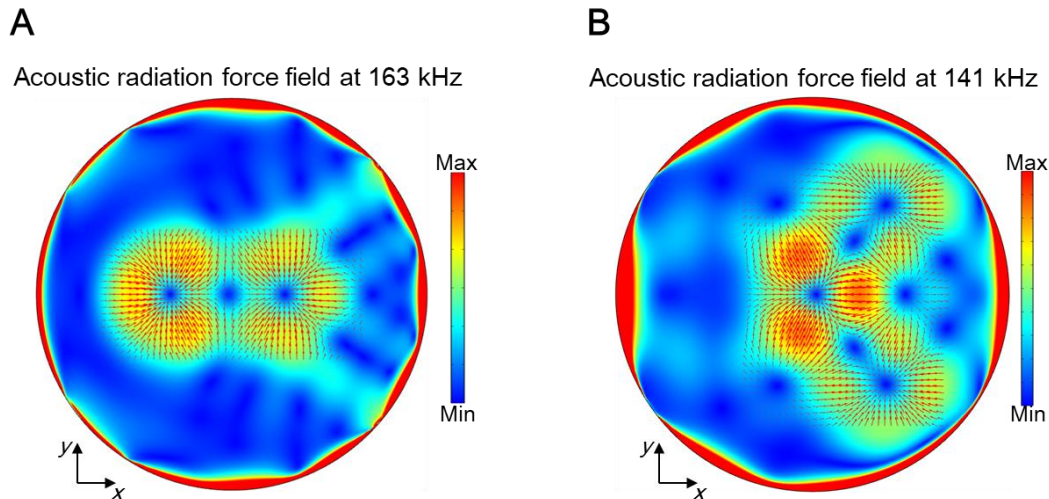


fig. S3. Simulated acoustic radiation force fields at different frequencies. (A) Simulation result at 163 kHz. (B) Simulation result at 141 kHz. For these simulations, 10- μm polystyrene particles at the droplet-substrate interface were used. The red arrows represent directions of acoustic radiation forces at different locations.

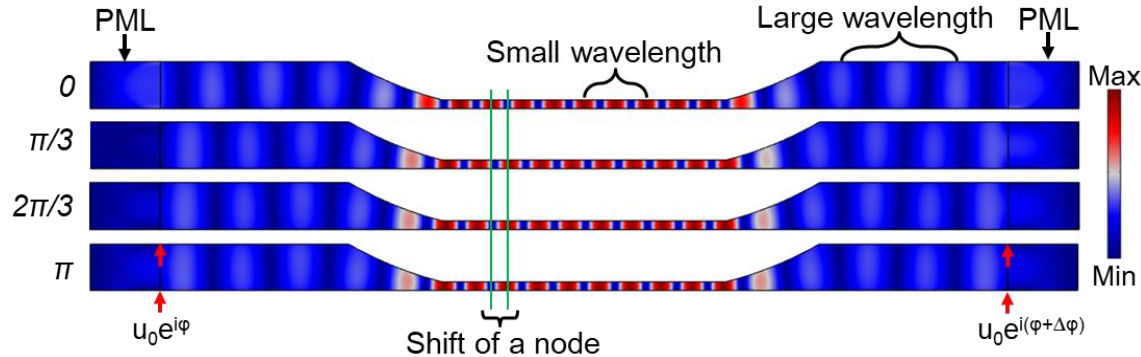


fig. S4. Simulated flexural wave fields showing the control of in-AFBH nodes. This simulation employs a 2D cross-sectional model, using an AFBH with an extended bottom diameter r_1 of 6 mm. Perfectly matched layers (PMLs) were placed at the left and right ends to eliminate reflections from substrate ends. The excitation frequency was 147 kHz. To generate pure flexural waves, point displacement-based excitations were used (illustrated by red arrows). The excitations applied to the left and right sides ($u_0e^{i\varphi}$ and $u_0e^{i(\varphi+\Delta\varphi)}$) have a phase difference of $\Delta\varphi$. Our simulation results show that waves in the AFBH have smaller wavelengths and higher intensities than those in areas outside the AFBH. Moreover, by changing the phase difference (from 0 to π), our simulation results show the in-AFBH node positions can be shifted.

Acoustic radiation force field at 147 kHz

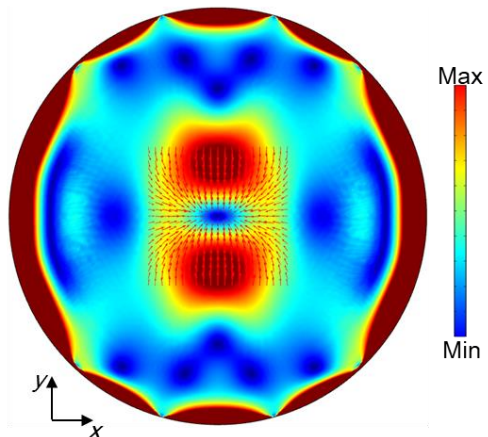


fig. S5. A simulated acoustic radiation force field for an AFBH between two transducers. For this simulation, the 10- μm polystyrene particles at the droplet-substrate interface were used. The simulation frequency was 147 kHz. The red arrows represent directions of acoustic radiation forces at different locations.

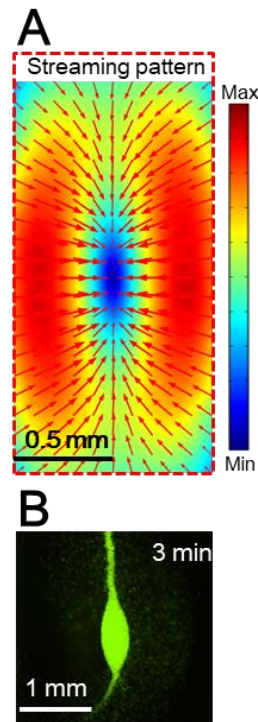


fig. S6. Simulation and experimental results for the single-site particle enrichment using our device. (A) A simulation result showing the acoustic streaming pattern around the enrichment area. **(B)** An acquired microscopy image showing that particles can be enriched by acoustic waves.

Acoustic radiation force field at 157 kHz

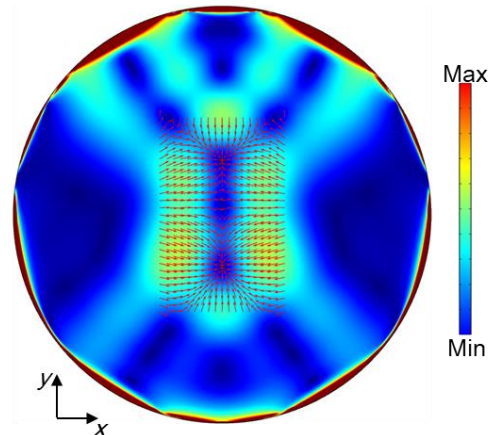


fig. S7. A simulated acoustic radiation force field for an AFBH of a circular AFBH array. For this simulation, the 10- μm polystyrene particles at the droplet-substrate interface were used. The simulation frequency was 157 kHz. The red arrows represent directions of acoustic radiation forces at different locations.

Displacement amplitude in the solid domain at 160 kHz

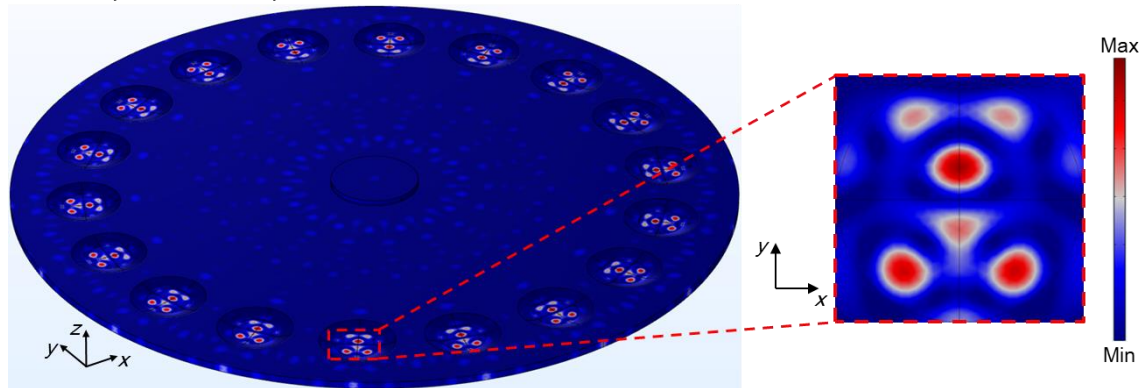


fig. S8. A simulated out-of-plane displacement amplitude field for flexural waves trapped by an array of 18 AFBHs. The simulation frequency was 160 kHz. This result indicates that our approach can trap flexural waves in multiple AFBHs. Moreover, the mode shapes in individual AFBHs are nearly the same suggesting our approach could potentially be used for high-throughput applications.

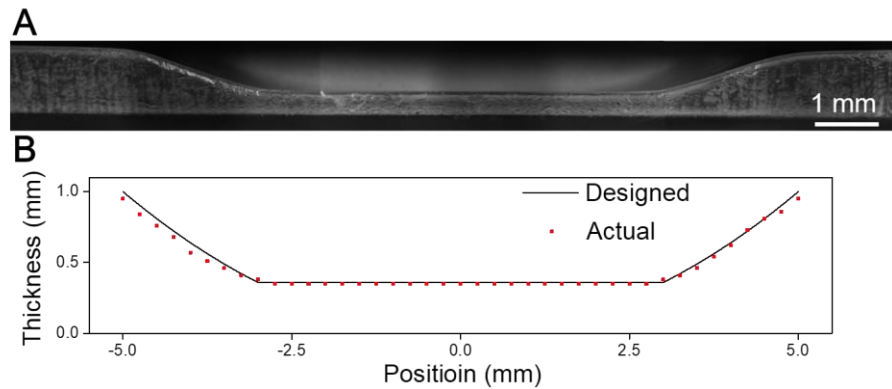


fig. S9. Material thickness characterization results for a PMMA substrate with an AFBH. (A) A captured cross-sectional image of a PMMA substrate with an AFBH. (B) Comparison between the wall profile of the fabricated substrate and the designed profile based on Eq. (1). From the comparison, it can be found that the thickness errors are less than 70 μm .

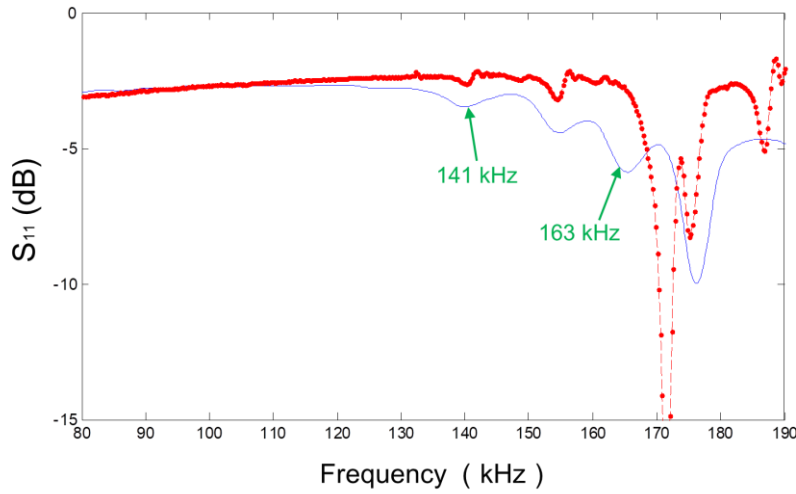


fig. S10. Reflection coefficient S_{II} curves for piezoelectric transducers. We measured the S_{II} curves for a free piezoelectric transducer (red dotted line) as well as a piezoelectric transducer bonded on an elliptical PMMA substrate (blue solid line) using a vector network analyzer (E5063A, Keysight). The S_{II} curve for a piezoelectric transducer bonded on an elliptical PMMA substrate shows multiple dips, including two dips near 141 kHz and 163 kHz.

table S1. Geometrical parameters for an AFBH.

h_1	0.36 mm
r_1	3 mm
a	0.04 mm ⁻¹
m	2
r_2	5 mm

table S2. Material properties used for numerical simulations.

Water	
Density	998.2 kg/m ³
Sound speed	1480 m/s
Dynamic viscosity	1.01 × 10 ⁻³ Pa·s
Bulk viscosity	2.82 × 10 ⁻³ Pa·s
Polystyrene particles	
Density	1050 kg/m ³
Sound speed	2350 m/s
PMMA plate	
Density	1190 kg/m ³
Young's modulus	3.2 GPa
Poisson's ratio	0.35
Isotropic loss factor	0.02
Epoxy	
Density	1673 kg/m ³
Young's modulus	1 GPa
Poisson's ratio	0.38
Isotropic loss factor	0.02

Legends for movies S1 to S3

movie S1. AFBH-based arrangement of 10- μm polystyrene particles at two antinodes in an AFBH. The experiment was performed using an AFBH-based elliptical-substrate device at a frequency of 163 kHz.

movie S2. AFBH-based arrangement of 10- μm polystyrene particles at three antinodes in an AFBH. The experiment was performed using an AFBH-based elliptical-substrate device at a frequency of 141 kHz.

movie S3. AFBH-based enrichment of 10- μm polystyrene particles at an antinode in an AFBH. The experiment was performed using a setup with an AFBH located between two circular piezoelectric transducers with the same excitation frequency of 147 kHz.

REFERENCES AND NOTES

1. L. H. Lin, E. H. Hill, X. L. Peng, Y. B. Zheng, Optothermal manipulations of colloidal particles and living cells. *Acc. Chem. Res.* **51**, 1465–1474 (2018).
2. L. Lin, M. S. Wang, X. L. Peng, E. N. Lissek, Z. M. Mao, L. Scarabelli, E. Adkins, S. Coskun, H. E. Unalan, B. A. Korgel, L. M. Liz-Marzan, E. L. Florin, Y. B. Zheng, Opto-thermoelectric nanotweezers. *Nat. Photonics* **12**, 195–201 (2018).
3. M. Hejazian, N. T. Nguyen, Magnetofluidic concentration and separation of non-magnetic particles using two magnet arrays. *Biomicrofluidics* **10**, 044103 (2016).
4. H. F. Feng, X. Xu, W. C. Hao, Y. Du, D. L. Tian, L. Jiang, Magnetic field actuated manipulation and transfer of oil droplets on a stable underwater superoleophobic surface. *Phys. Chem. Chem. Phys.* **18**, 16202–16207 (2016).
5. T. Y. Zheng, Z. Z. Zhang, R. Zhu, Flexible trapping and manipulation of single cells on a chip by modulating phases and amplitudes of electrical signals applied onto microelectrodes. *Anal. Chem.* **91**, 4479–4487 (2019).
6. S. Park, Y. Zhang, T. H. Wang, S. Yang, Continuous dielectrophoretic bacterial separation and concentration from physiological media of high conductivity. *Lab Chip* **11**, 2893–2900 (2011).
7. M. Moreno-Moreno, P. Ares, C. Moreno, F. Zamora, C. Gomez-Navarro, J. Gomez-Herrero, AFM manipulation of gold nanowires to build electrical circuits. *Nano Lett.* **19**, 5459–5468 (2019).
8. H. Z. Liu, S. Wu, J. M. Zhang, H. T. Bai, F. Jin, H. Pang, X. D. Hu, Strategies for the AFM-based manipulation of silver nanowires on a flat surface. *Nanotechnology* **28**, 365301 (2017).
9. W. Connacher, N. Q. Zhang, A. Huang, J. Y. Mei, S. Zhang, T. Gopesh, J. Friend, Micro/nano acoustofluidics: Materials, phenomena, design, devices, and applications. *Lab Chip* **18**, 1952–1996 (2018).

10. J. Friend, L. Y. Yeo, Microscale acoustofluidics: Microfluidics driven via acoustics and ultrasonics. *Rev. Mod. Phys.* **83**, 647–704 (2011).
11. A. Ozcelik, J. Rufo, F. Guo, Y. Y. Gu, P. Li, J. Lata, T. J. Huang, Acoustic tweezers for the life sciences. *Nat. Methods* **15**, 1021–1028 (2018).
12. K. Melde, A. G. Mark, T. Qiu, P. Fischer, Holograms for acoustics. *Nature* **537**, 518–522 (2016).
13. M. Baudoin, J. C. Gerbedoen, A. Riaud, O. B. Matar, N. Smagin, J. L. Thomas, Folding a focalized acoustical vortex on a flat holographic transducer: Miniaturized selective acoustical tweezers. *Sci. Adv.* **5**, eaav1967 (2019).
14. V. Pereno, M. Aron, O. Vince, C. Mannaris, A. Seth, M. de Saint Victor, G. Lajoinie, M. Versluis, C. Coussios, D. Carugo, E. Stride, Layered acoustofluidic resonators for the simultaneous optical and acoustic characterisation of cavitation dynamics, microstreaming and biological effects. *Biomicrofluidics* **12**, 034109 (2018).
15. L. Y. Yeo, H. C. Chang, P. P. Y. Chan, J. R. Friend, Microfluidic devices for bioapplications. *Small* **7**, 12–48 (2011).
16. P. Li, T. J. Huang, Applications of acoustofluidics in bioanalytical chemistry. *Anal. Chem.* **91**, 757–767 (2019).
17. L. Moroni, J. A. Burdick, C. Highley, S. J. Lee, Y. Morimoto, S. Takeuchi, J. J. Yoo, Biofabrication strategies for 3D in vitro models and regenerative medicine. *Nat. Rev. Mater.* **3**, 21–37 (2018).
18. B. Su, Y. C. Wu, L. Jiang, The art of aligning one-dimensional (1D) nanostructures. *Chem. Soc. Rev.* **41**, 7832–7856 (2012).
19. Z. Y. He, N. Ranganathan, P. Li, Evaluating nanomedicine with microfluidics. *Nanotechnology* **29**, 492001 (2018).

20. L. Y. Zhang, Z. H. Tian, H. Bachman, P. R. Zhang, T. J. Huang, A cell-phone-based acoustofluidic platform for quantitative point-of-care testing. *ACS Nano* **14**, 3159–3169 (2020).
21. N. J. Hao, Z. C. Pei, P. Z. Liu, H. Bachman, T. D. Naquin, P. R. Zhang, J. X. Zhang, L. Shen, S. J. Yang, K. C. Yang, S. G. Zhao, T. J. Huang, Acoustofluidics-assisted fluorescence-SERS bimodal biosensors. *Small* **16**, 2005179 (2020).
22. H. Sazan, S. Piperno, M. Layani, S. Magdassi, H. Shpaisman, Directed assembly of nanoparticles into continuous microstructures by standing surface acoustic waves. *J. Colloid Interface Sci.* **536**, 701–709 (2019).
23. M. K. Nichols, R. K. Kumar, P. G. Bassindale, L. F. Tian, A. C. Barnes, B. W. Drinkwater, A. J. Patil, S. Mann, Fabrication of micropatterned dipeptide hydrogels by acoustic trapping of stimulus-responsive coacervate droplets. *Small* **14**, 1800739 (2018).
24. P. R. Zhang, H. Bachman, A. Ozcelik, T. J. Huang, Acoustic microfluidics. *Annu. Rev. Anal. Chem.* **13**, 17–43 (2020).
25. X. Y. Ding, P. Li, S. C. S. Lin, Z. S. Stratton, N. Nama, F. Guo, D. Slotcavage, X. L. Mao, J. J. Shi, F. Costanzo, T. J. Huang, Surface acoustic wave microfluidics. *Lab Chip* **13**, 3626–3649 (2013).
26. Y. L. Xie, H. Bachman, T. J. Huang, Acoustofluidic methods in cell analysis. *TrAC Trends Anal. Chem.* **117**, 280–290 (2019).
27. V. Bussiere, A. Vigne, A. Link, J. McGrath, A. Srivastav, J. C. Baret, T. Franke, High-throughput triggered merging of surfactant-stabilized droplet pairs using traveling surface acoustic waves. *Anal. Chem.* **91**, 13978–13985 (2019).
28. J. Reboud, C. Auchinbole, C. D. Syme, R. Wilson, J. M. Cooper, Acoustically controlled enhancement of molecular sensing to assess oxidative stress in cells. *Chem. Commun.* **49**, 2918–2920 (2013).

29. D. J. Collins, B. Morahan, J. Garcia-Bustos, C. Doerig, M. Plebanski, A. Neild, Two-dimensional single-cell patterning with one cell per well driven by surface acoustic waves. *Nat. Commun.* **6**, 8686 (2015).
30. G. Destgeer, H. Cho, B. H. Ha, J. H. Jung, J. Park, H. J. Sung, Acoustofluidic particle manipulation inside a sessile droplet: Four distinct regimes of particle concentration. *Lab Chip* **16**, 660–667 (2016).
31. D. J. Collins, Z. C. Ma, J. Han, Y. Ai, Continuous micro-vortex-based nanoparticle manipulation via focused surface acoustic waves. *Lab Chip* **17**, 91–103 (2017).
32. Y. Y. Gu, C. Y. Chen, Z. M. Mao, H. Bachman, R. Becker, J. Rufo, Z. Y. Wang, P. R. Zhang, J. Mai, S. J. Yang, J. X. Zhang, S. G. Zhao, Y. S. Ouyang, D. T. W. Wong, Y. Sadovsky, T. J. Huang, Acoustofluidic centrifuge for nanoparticle enrichment and separation. *Sci. Adv.* **7**, eabc0467 (2021).
33. Z. H. Tian, S. J. Yang, P. H. Huang, Z. Y. Wang, P. R. Zhang, Y. Y. Gu, H. Bachman, C. Y. Chen, M. X. Wu, Y. B. Xie, T. J. Huang, Wave number-spiral acoustic tweezers for dynamic and reconfigurable manipulation of particles and cells. *Sci. Adv.* **5**, eaau6062 (2019).
34. D. Carugo, T. Octon, W. Messaoudi, A. L. Fisher, M. Carboni, N. R. Harris, M. Hill, P. Glynne-Jones, A thin-reflector microfluidic resonator for continuous-flow concentration of microorganisms: A new approach to water quality analysis using acoustofluidics. *Lab Chip* **14**, 3830–3842 (2014).
35. A. Ku, H. C. Lim, M. Evander, H. Lilja, T. Laurell, S. Scheding, Y. Ceder, Acoustic enrichment of extracellular vesicles from biological fluids. *Anal. Chem.* **90**, 8011–8019 (2018).
36. A. E. Christakou, M. Ohlin, B. Onfelt, M. Wiklund, Ultrasonic three-dimensional on-chip cell culture for dynamic studies of tumor immune surveillance by natural killer cells. *Lab Chip* **15**, 3222–3231 (2015).

37. P. Augustsson, J. T. Karlsen, H. W. Su, H. Bruus, J. Voldman, Iso-acoustic focusing of cells for size-insensitive acousto-mechanical phenotyping. *Nat. Commun.* **7**, 11556 (2016).
38. B. W. Drinkwater, Dynamic-field devices for the ultrasonic manipulation of microparticles. *Lab Chip* **16**, 2360–2375 (2016).
39. J. Hu, *Ultrasonic Micro/Nano Manipulations: Principles and Examples* (World Scientific, 2014).
40. A. D. Maxwell, M. Bailey, B. W. Cunitz, M. Terzi, A. Nikolaeva, S. Tsysar, O. A. Sapozhnikov, Vortex beams and radiation torque for kidney stone management. *J. Acoust. Soc. Am.* **139**, 2040–2040 (2016).
41. J. Reboud, Y. Bourquin, R. Wilson, G. S. Pall, M. Jiwaji, A. R. Pitt, A. Graham, A. P. Waters, J. M. Cooper, Shaping acoustic fields as a toolset for microfluidic manipulations in diagnostic technologies. *Proc. Natl. Acad. Sci. U.S.A.* **109**, 15162–15167 (2012).
42. R. Wilson, J. Reboud, Y. Bourquin, S. L. Neale, Y. Zhang, J. M. Cooper, Phononic crystal structures for acoustically driven microfluidic manipulations. *Lab Chip* **11**, 323–328 (2011).
43. Y. Y. Gu, C. Y. Chen, J. Rufo, C. Shen, Z. Y. Wang, P. H. Huang, H. Fu, P. R. Zhang, S. A. Cummer, Z. H. Tian, T. J. Huang, Acoustofluidic holography for micro- to nanoscale particle manipulation. *ACS Nano* **14**, 14635–14645 (2020).
44. Z. C. Ma, A. W. Holle, K. Melde, T. Qiu, K. Poeppel, V. M. Kadiri, P. Fischer, Acoustic holographic cell patterning in a biocompatible hydrogel. *Adv. Mater.* **32**, 1904181 (2020).
45. R. M. Wald, *General Relativity* (University of Chicago Press, 1984).
46. A. Pelat, F. Gautier, S. C. Conlon, F. Semperlotti, The acoustic black hole: A review of theory and applications. *J. Sound Vib.* **476**, 115316 (2020).
47. V. V. Krylov, Acoustic black holes: Recent developments in the theory and applications. *IEEE Trans. Ultrason. Ferroelectr. Freq. Control* **61**, 1296–1306 (2014).

48. B. W. Drinkwater, An acoustic black hole. *Nat. Phys.* **16**, 1010–1011 (2020).
49. V. Giurgiutiu, *Structural Health Monitoring with Piezoelectric Wafer Active Sensors* (Elsevier Inc., Academic Press, ed. 2, 2014).
50. V. V. Krylov, F. J. B. S. Tilman, Acoustic ‘black holes’ for flexural waves as effective vibration dampers. *J. Sound Vib.* **274**, 605–619 (2004).
51. L. X. Zhao, S. C. Conlon, F. Semperlotti, An experimental study of vibration based energy harvesting in dynamically tailored structures with embedded acoustic black holes. *Smart Mater. Struct.* **24**, 065039 (2015).
52. J. J. Lei, Formation of inverse Chladni patterns in liquids at microscale: Roles of acoustic radiation and streaming-induced drag forces. *Microfluid. Nanofluid.* **21**, 50 (2017).
53. G. Vuillermet, P. Y. Gires, F. Casset, C. Poulain, Chladni patterns in a liquid at microscale. *Phys. Rev. Lett.* **116**, 184501 (2016).
54. P. Z. Liu, Z. H. Tian, N. J. Hao, H. Bachman, P. R. Zhang, J. H. Hu, T. J. Huang, Acoustofluidic multi-well plates for enrichment of micro/nano particles and cells. *Lab Chip* **20**, 3399–3409 (2020).
55. Z. M. Mao, P. Li, M. X. Wu, H. Bachman, N. Mesyngier, X. S. Guo, S. Liu, F. Costanzo, T. J. Huang, Enriching nanoparticles via acoustofluidics. *ACS Nano* **11**, 603–612 (2017).
56. A. F. Bower, *Applied Mechanics of Solids* (CRC Press, 2009).
57. D. T. Blackstock, *Fundamentals of Physical Acoustics* (Wiley-Interscience, 2000).
58. L. E. Kinsler, A. R. Frey, A. B. Coppens, J. V. Sanders, *Fundamentals of Acoustics* (Wiley, ed. 4, 1999).
59. Q. Tang, J. H. Hu, Analyses of acoustic streaming field in the probe-liquid-substrate system for nanotrapping. *Microfluid. Nanofluid.* **19**, 1395–1408 (2015).

60. L. P. Gor'kov, On the forces acting on a small particle in an acoustical field in an ideal fluid. *Soviet Phys. Dokl.* **6**, 773–775 (1962).
61. W. L. Nyborg, Acoustic streaming due to attenuated plane waves. *J. Acoust. Soc. Am.* **25**, 68–75 (1953).
62. J. Lighthill, Acoustic streaming. *J. Sound Vib.* **61**, 391–418 (1978).
63. P. Z. Liu, Q. Tang, S. F. Su, J. H. Hu, Principle analysis for the micromanipulation probe-type ultrasonic nanomotor. *Sens. Actuators A* **318**, 112524 (2021).
64. Q. Tang, P. Z. Liu, J. H. Hu, Analyses of acoustofluidic field in ultrasonic needle-liquid-substrate system for micro-/nanoscale material concentration. *Microfluid. Nanofluid.* **22**, 46 (2018).
65. P. F. Zhu, J. H. Hu, Modeling and analysis of the droplet-ultrasonic stage system for nano concentration. *Sens. Actuators A* **225**, 111–118 (2015).